Iron isotopes suggestreveal significant aerosol dissolution over the Pacific Ocean

Authors: Capucine Camin[1], François Lacan[1], Catherine Pradoux[1], Marie Labatut[1], Anne Johansen[2], James W. Murray[3]

[1] UNIVERSITE DE TOULOUSE, LEGOS (CNES/CNRS/IRD/UT3), TOULOUSE, FRANCE
[2] CENTRAL WASHINGTON UNIVERSITY, ELLENSBURG, WASHINGTON, USA
[3] SCHOOL OF OCEANOGRAPHY, UNIVERSITY OF WASHINGTON, SEATTLE, WASHINGTON, USA

Corresponding authors: Camin C. and Lacan F., LEGOS, 14 Avenue Edouard Belin, F-31400 Toulouse, France (capucine.camin@orange.fr and francois.lacan@cnrs.fr).

Abstract

This study presents aerosol iron isotopic compositions (δ^{56}Fe) in Western and Central Equatorial and Tropical Pacific Ocean. Aerosols supply iron (Fe), a critical element for marine primary production, to the open ocean. Particulate aerosols, $> 1\,\mu$m, were sampled during EUCFe (Equatorial Undercurrent Fe) cruise (RV *Kilo Moana*, PI: J. W. Murray, 2006). One aerosol sample was isotopically lighter than the crust (δ^{56}Fe=-0.16 ± 0.07 ‰, 95 % confidence interval), possibly originating from combustion processes. The nine other aerosol samples were isotopically heavier than the crust, with a rather homogeneous signature of +0.31 ± 0.21 ‰ (2SD, n=9). Given i) this homogeneity compared to the diversity of their modeled geographic origin and ii) the values of the Fe/Ti ratios used as a lithogenic tracer, we suggest that these heavy δ^{56}Fe signatures reflect isotopic fractionation of crustal aerosols caused by atmospheric processes. Using a fractionation factor of $\Delta_{\text{solution - particle}}$=-1.8~~1~~ ‰, a partial dissolution of $\approx 13\text{\sout{20}}$ % of the initial aerosol iron content, followed by the removal of this dissolved fraction, would explain the observed slightly heavy Fe isotope signatures. Such fractionation has been observed previously in laboratory experiments, but never before in a natural environment. The removal of the dissolved fraction of the aerosols has not been previously documented either. This work illustrates the strong constrains provided by the use of iron isotopes for atmospheric process studies.

Key words: Iron Isotopes, Aerosols, Equatorial and Tropical Pacific, Partial Dissolution, Fractionation

Graphical Abstract
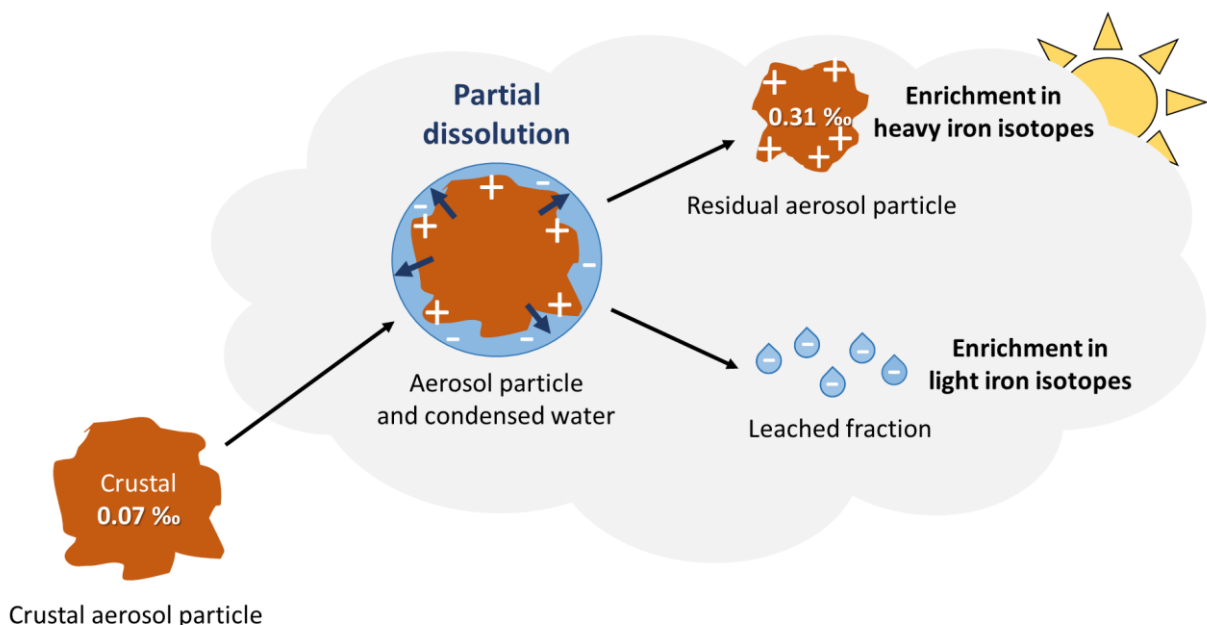
Key points
- Iron isotope fractionation of particle aerosol during atmospheric transport
- Preferential dissolution and subsequent removal of the dissolved fraction

2

1. INTRODUCTION

Iron (Fe) is an essential micronutrient for phytoplankton, playing a key role in primary production, nitrogen fixation and community structures (Boyd and Ellwood, 2010; Morel et al., 2020). Availability and speciation of this micronutrient impact the global carbon cycle and climate. In some areas of the open ocean, low concentrations of Fe can limit primary production (Martin, 1992). Five predominant sources of bioavailable Fe to the global ocean are currently thought to be aerosol dissolution (Duce and Tindale, 1991; Jickells et al., 2005; Moore and Braucher, 2008), sediment dissolution and resuspension (Elrod et al., 2004; Radic et al., 2011; Labatut et al., 2014), fluvial inputs (Poulton and Raiswell, 2002), hydrothermal vents (Tagliabue et al., 2010; Resing et al., 2015) and locally ice melting (Raiswell et al., 2008). Iron sources to the open ocean remain insufficiently understood.

Over the past two decades For about twenty years, it has become possible to measure iron isotopes in the environment. The isotopic composition is expressed by δ^{56}Fe in ‰ which shows the deviation of the sample's ^{56}Fe/^{54}Fe ratio relative to the reference material IRMM-14 (Eq. 1):

$$\delta^{56}\text{Fe} = \frac{\left(^{56}\text{Fe}/^{54}\text{Fe}\right)_{\text{sample}}}{\left(^{56}\text{Fe}/^{54}\text{Fe}\right)_{\text{IRMM}-14}} - 1 \qquad (1)$$

With this definition, the upper continental crust is characterized by an homogeneous signature of δ^{56}Fe = +0.07 ‰ (Poitrasson, 2006). Iron isotopes measurements have led to significant advances in our understanding of the cycle of this element (Radic et al., 2011; John et al., 2012; Conway and John, 2014; Ellwood et al., 2015; Abadie et al., 2017; Klar et al., 2018; Chen et al., 2020; Homoky et al., 2021). However, isotopic studies on aerosols in marine environments are still very rare.

Aerosols can be of natural or anthropogenic origins, each associated with variable ranges of Fe isotope signatures (Wang et al., 2022). Natural sources of aerosols are rocks, soils, loess, seawater, river water, volcanoes, plants, and biomass burning. For instance, lithogenic sources Fe isotopic compositions are in a narrow range between -0.11 ‰ and +0.12 ‰ (Beard et al., 2003). Anthropogenic aerosols are mainly derived from combustion processes such as coal combustion, metallurgy, waste incineration and vehicle exhaust (Kommalapati and Valsaraj, 2009). These aerosols have been found to span a large range of δ^{56}Fe values, from -3.91 ‰ (Kurisu et al., 2016b) to +0.80 ‰ (Flament et al., 2008). Therefore, iron isotopes can be used to identify aerosol sources. Nevertheless, initial aerosol isotope signatures may be modified through isotope fractionations during atmospheric transport. Such fractionation can complicate interpretation of isotopic signatures as source tracers. Laboratory experiments have documented Fe isotope fractionation due to aerosol partial dissolution (Mulholland et al., 2021; Maters et al., 2022). However, such fractionation has not been evidenced from in situ data. This is only one potential explanation among others to understand iron isotope signature of aerosols during field study (Kurisu et al., 2021). Aerosol Fe isotopic data are scarce in oceanic environments, and none have been reported in the Equatorial Pacific, despite the important role of iron as a limiting micronutrient in the Eastern Equatorial Pacific.

This article presents iron isotope data from these aerosols collected in the Equatorial and Tropical Pacific. Combined with elemental concentration data and modeled back trajectories, these isotopic data provide new constraints on the processes involved in the aerosol iron cycle during their transport.

2. SAMPLING LOCATIONS AND METHODS
2.1. AEROSOL SAMPLING

Atmospheric particles were sampled during the EUCFe cruise (August – October 2006, R/V *Kilo Moana*, Chief Scientist J. W. Murray). This cruise was carried out to study the iron cycle, including atmospheric deposition, in the Equatorial and Tropical Pacific (Slemons et al., 2009, 2010, 2012; Radic et al., 2011; Labatut et al., 2014). Samples were collected along the cruise track with a small volume collector equipped with 1 µm porosity 47 mm diameter PTFE membranes, placed in a Millipore® polycarbonate filter holder. The membranes were pre-

cleaned had previously been acid cleaned with in ultrapure HNO_3 for 2 days and stored in clean
plastic Petri dishes. The collector was located on the top deck and equipped with a control
system to stop pumping when the wind came from a direction greater than 60 ° from the bow
to prevent ship smoke collection. To protect the samples from rain, the filter support was angled
downwards and covered with a plastic protector. A flow meter provided information on the
pumped air flow: 8 L min^{-1} for A281 and A284 samples and 28 L min^{-1} for the eight other
samples. Each sample was collected over a duration of 3 days on average, for sample size
ranging between 9 and 93 m^3 (from coastal to open ocean areas). The sampling locations are
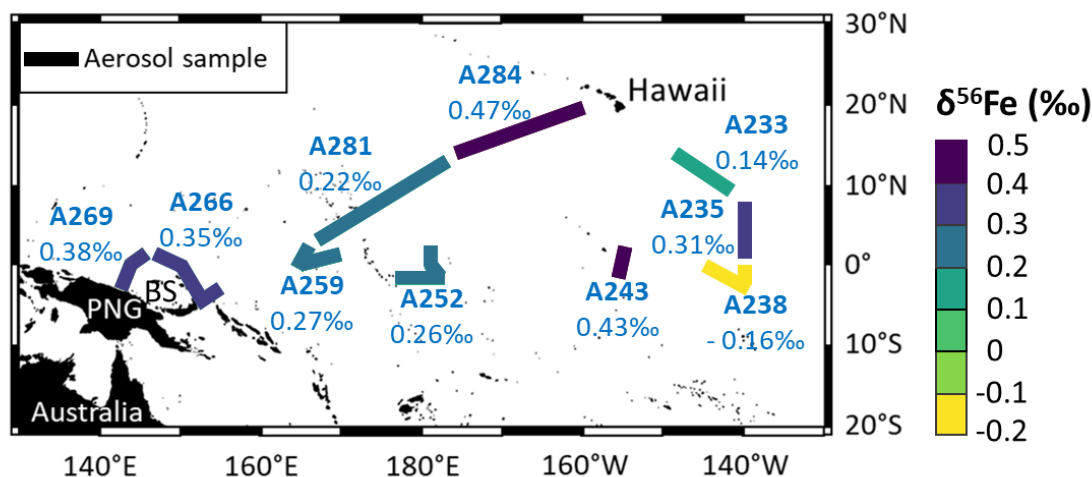reported in Fig. 1. The sampling area is more than 8,000 km wide.

Figure 1. Location of aerosol samples. Aerosol sampling transects are shown by the thick lines.
The Fe isotopic compositions are indicated by the color bar and under the sample names. PNG
stands for Papua New Guinea. BS stands for Bismarck Sea.

Three samples previously published close to the Bismarck Sea and in the Equatorial Pacific are
reported to enrich the discussion: A269, A266 and A259 (Fig. 1 and Table 3) (Labatut et al.,
2014).

2.2. ANALYTICAL PROCEDURE

The elemental concentrations and iron isotopic compositions were measured at LEGOS
laboratory (Observatoire Midi-Pyrénées, Toulouse, France), in the years 2009 to 2012. The
analytical procedure was described by Labatut et al. (2014) and is summarized here. A trace
metal clean laboratory, an ISO4 laminar flow hood, high purity reagents and acid cleaned
labware were used for all chemical procedures. The particles were totally digested using a
mixture of 5 M HCl, 2.1 M HNO_3 and 0.6 M HF at 130 °C. To check that the procedure was
quantitative, some filters were digested twice a second time and no particulate Fe PFe was
detected in the second leach. A ^{57}Fe-^{58}Fe double spike was added to the leachates. 2 % aliquots
were taken for multi-elemental concentration determination on an ThermoScientific Element-
XR HR-ICP-MS. Na, Mg, Al, Ca, Ti, Fe, V, Zn, Rb, Sr, Ba, La, Ce and Pb concentrations were
quantified. Fe was purified from the remaining 98 % with an AG® 1-X4 anionic resin, and its
isotopic composition and concentration measured on a ThermoScientific Neptune MC-ICPMS.
    Throughout this article, uncertainties are given at a 95 % confidence level. For the Fe
concentration and isotope measurements on the Neptune, the total procedural recovery was
93 ± 25 %. Total procedural blank, including contamination from the sampling filter, was
3.0 ng, which was 3.8 and 14.7 % of the average and smallest sample, respectively.
Repeatability was not determined on aerosol samples but was quantified during the same
measurement sessions from duplicate analyses, including distinct chemical treatments, of four
seawater suspended particle samples due to insufficient samples for duplicate analysis. It was
4 % and 0.04 ‰ for concentration and isotopic composition, respectively. This repeatability for

δ^{56}Fe is better than the long-term external precision of 0.07 ‰ of our measurements, determined from repeated analysis of a secondary isotopic standard (an in-house "hematite" standard). The uncertainties characterizing our Fe isotope data are therefore 0.07 ‰ or the internal measurement uncertainty (2 standard errors), when the latter is larger. The iron isotope protocol at LEGOS has been validated through intercalibration and intercomparison exercises (Boyle et al., 2012; Conway et al., 2016) and described in Lacan et al. (2008, 2010, 2021). The in-house "ETH-Hematite" standard displayed an isotopic composition of +0.52 ± 0.08 ‰ (2SD, n=81), which was perfectly consistent with the recommended value of +0.53 ± 0.06 ‰ (2SD, n=6) (Lacan et al., 2010). We also measured the sediment geostandard GBW 07315 with δ^{56}Fe = +0.04 ± 0.046 ‰. Unfortunately, it is not certified for Fe isotopes and we could not find Fe isotope values reported in the literature. We still report it here as it could be useful in the future. Trueness of concentrations determined by HR-ICPMS analysis was verified using certified SLRS-5 river water material and GBW 07315 sediment material. The accuracy quality (trueness and repeatability) of our HR-ICPMS concentration determination was also validated through intercalibration exercises (Yeghicheyan et al., 2013, 2019). Blanks were quantified for Fe only. Based on the latter measured Fe blank, and assuming a crustal composition for aerosols, they were estimated for the other elements. This assumption is supported by the lack of contamination discussed in Sect. 3.1. below. This leads to blank levels are always lower than 15 % of each sample and all elements, except for Ca for which it was 11.8 % on average and 35.7 % maximum.

2.3. HYSLIPT MODEL

To identify the origin of sampled aerosols, air mass back trajectories were calculated using the NOAA Hybrid Single-Particle Lagrangian Integrated Trajectory (HYSPLIT) model (Stein et al., 2015). The meteorological data selected was the Global Data Assimilation System (GDAS). Trajectories were computed at 50 m above ground level with a 7.5 days run time. Aerosol samplings were conducted between 22 August and 12 October 2006. In order to represent spatial and temporal variabilities and to present a synthetic overview, we divided the cruise track in four areas (Fig. 2).
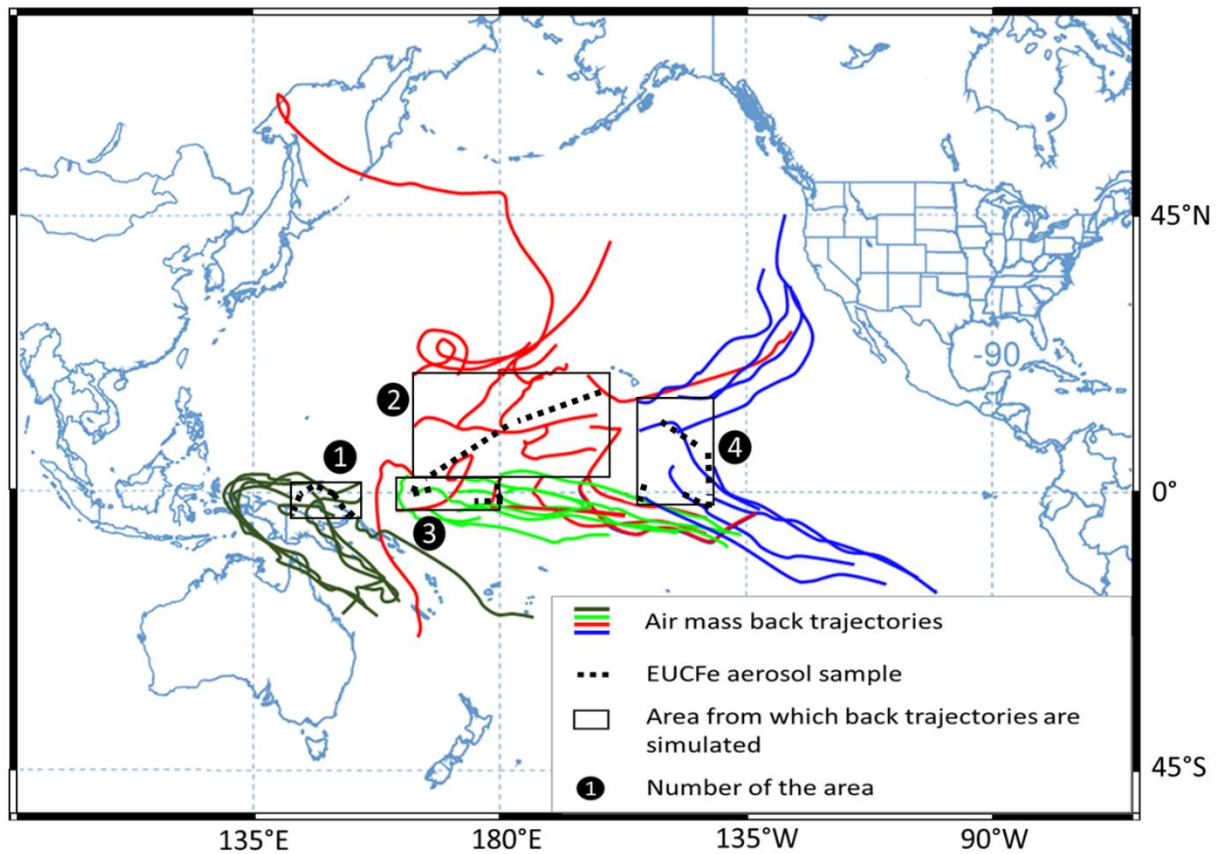
Figure 2. Air mass back trajectories (colors lines) calculated with Hybrid Single-Particle Lagrangian Integrated Trajectory model (HYSPLIT, NOAA, GDSA Meteorological Data). Trajectories were conducted at the height of 50 m (AGL) with a 7.5 days run time. Each color is associated with an area from which back trajectories are simulated. Air mass back trajectories' colors are only used for easier understanding.

For each area from which back trajectories are simulated, the starting points of back trajectories were chosen as a grid for representativity and clarity purposes. The grid points are not precisely sampling locations but they are close to them. The starting times were chosen as the central dates between the sampling period of each area (Table 1).

Table 1. Parameters selected for the HYSPLIT model simulations and the aerosol sample names within areas from which back trajectories are simulated.

Area Number	Area – Lower left grid point	Area – Upper right grid point	Number of starting points within the area	Starting time	Aerosol samples within the area
1	142° E 4° S	154° E 2° N	9	25 September 2006, 16:00:00 UTC	A266, A269
2	164° E 3° N	160° W 21° N	15	11 October 2006, 16:00:00 UTC	A281, A284
3	164° E 3° S	180° 3° N	9	13 September 2006, 16:00:00 UTC	A252, A259
4	155° W 1° S	139° W 15° N	12	26 August 2006, 16:00:00 UTC	A233, A235, A238, A243

6

3. RESULTS

Elemental concentrations are presented in Table 2. Isotopic compositions of Fe in aerosols are reported in Table 3 and in Fig. 1.

Table 2. Aerosol elemental concentrations from the EUCFe cruise. Concentration uncertainty was 4 % (95 % confidence level). Some concentrations were found below quantification limits. In that case, they are reported after the "<" symbol. The mean concentrations do not take into account samples with concentration below quantification limits. Al concentrations for A252 sample (reported in brackets in the table) was suspected to be contaminated, it is not included in the mean calculation and in the discussion. UCC stands for Upper Continental Crust. Note that the different detection limits for the same element are due to different sample volumes (m^3).

Samples	[Na] ng m⁻³	[Mg] ng m⁻³	[Ca] ng m⁻³	[Sr] pg m⁻³	[Ba] pg m⁻³	[Al] ng m⁻³	[Ti] ng m⁻³	[V] pg m⁻³	[Fe] ng m⁻³	~~[Ho] pg m⁻³~~	~~[Ce] pg m⁻³~~	~~[Zn] pg m⁻³~~	[Rb] pg m⁻³	[Pb] pg m⁻³
A233	135	17.5	13.4	170	37.4	2.42	0.30	5.91	1.71	~~0.43~~	~~1.20~~	~~798~~	<22.3	11.1
A235	1 085	128	64.9	1 144	28.2	1.90	0.73	7.09	7.22	~~0.59~~	~~1.78~~	~~3 795~~	13.5	14.4
A238	3 031	323	126	2 169	272	20.3	0.59	13.4	3.81	~~1.57~~	~~4.59~~	~~786~~	58.7	17.2
A243	1 021	114	49.0	730	372	26.1	0.50	<49.9	2.28	~~0.99~~	~~1.78~~	~~1 143~~	45.5	<63.2
A252	2 432	223	85.4	1 552	68.2	(188)	0.22	64.9	0.99	~~0.48~~	~~0.71~~	~~749~~	20.5	13.9
A259	809	77.6	36.1	520	<40.9	0.76	0.20	4.77	0.38	~~0.68~~	~~1.28~~	~~624~~	<28.8	10.7
A266	224	20	8.93	<91.4	<18.6	1.28	0.12	<12.6	5.56	~~<4.15~~	~~<4.21~~	~~<407~~	<13.1	<16.0
A269	121	12.5	4.94	84.6	17.9	2.19	0.11	<16.6	0.54	~~0.62~~	~~1.17~~	~~387~~	<17.2	19.9
A281	653	58.6	26.0	373	75.0	9.15	0.42	20.9	2.42	~~1.24~~	~~2.97~~	~~795~~	<41.1	29.5
A284	1 072	97.7	41.5	652	418	23.5	0.45	28.4	5.17	~~2.42~~	~~8.51~~	~~1 633~~	50.3	41.8
Mean concentrations of samples	1 058	107	45.6	822	161	9.7	0.36	20.8	3.01	~~1.00~~	~~2.66~~	~~1 190~~	38	19.8
Mean UCC in g g⁻¹ (Rudnick and Gao, 2014)	2.43×10^{-2}	1.50	2.57	3.20×10^{-4}	6.24×10^{-4}	8.15×10^{-2}	3.84×10^{-3}	9.70×10^{-5}	3.92×10^{-2}	~~3.10×10^{-5}~~	~~6.30×10^{-5}~~	~~6.70×10^{-5}~~	8.40×10^{-5}	1.70×10^{-5}
Typical North Pacific concentrations in filtered seawater in ng kg⁻¹ (Nozaki, 1997)	1.08×10^{10}	1.28×10^{9}	4.12×10^{8}	7.80×10^{6}	1.50×10^{4}	30.0	6.50	2.00×10^{3}	30.0	5.60	0.70	~~3.50×10^{-2}~~	1.20×10^{5}	2.70

Table 3. Aerosol Fe isotopic compositions during the EUCFe cruise. U95 stands for measurement uncertainty at the 95 % confidence level. (*) identifies data previously published by Labatut et al. (2014).

Samples ID	Location	Sampling date	δ^{56}Fe (‰)	δ^{56}Fe U95 (‰)
A233	from 12.39° N 149.54° W to 06.01° N 143.42° W	21-23/08/2006	+0.14	0.07
A235	from 06.01° N 143.42° W to 01.07° N 140.00° W	23-25/08/2006	+0.31	0.07
A238	from 00.0° N 140.0° W to 00.52° S 144.15° W	26-28/08/2006	-0.16	0.07
A243	from 01.02° N 154.60° W to 01.31° S 155.00° W	31/08-01/09/2006	+0.43	0.07
A252	from 02.02° N 180.00° E to 01.22° S 178.16° E	09-11/09/2006	+0.26	0.07
A259*	from 01.48° N 167.31° E to 01.06° N 164.59° E	16-17/09/2006	+0.27	0.15
A266*	from 02.32° S 153.56° E to 01.18° N 146.34° E	23-25/09/2006	+0.35	0.07
A269*	from 01.18° N 146.33° E to 03.21° S 143.52° E	26-28/09/2006	+0.38	0.08
A281	from 03.39° N 167.55° E to 13.02° N 175.06° W	08-11/10/2006	+0.22	0.09
A284	from 14.20° N 173.5° W to 20.20° N 160.50° W	11-14/10/2006	+0.47	0.08

3.1. ELEMENTAL CONCENTRATIONS

Aerosol iron concentrations ranged from 0.38 ± 0.02 ng m^{-3} to 7.22 ± 0.28 ng m^{-3} (Table 2). Excluding aerosol sample A266 close to the Bismarck Sea (5.56 ± 0.22 ng m^{-3}), concentrations vary from low values (< 1 ng m^{-3}) between 140° E and 160° W along the equator to large values (> 1.5 ng m^{-3} and < 8 ng m^{-3}) in the North Tropical Pacific region and between 160°W and 140°W along the equator. There was no correlation between distance from land and concentration. A major volcanic eruption of Tavurvur (Papua New Guinea) occurred on 7 October 2006 (Wunderman, 2006). Samples A233 to A269 were collected prior to this event and are therefore unaffected. While it is theoretically possible that samples A281 and A284 could have been influenced by the eruption, they were collected over 1,500 km away from the volcano. A simulation of the forward trajectory of air masses confirms that samples A281 and A284 were not affected by the eruption (Fig. A1 and Fig. A2). Additionally, their concentrations are consistent with those of samples collected before the eruption, confirming that they were not impacted.

Aerosols Fe concentrations in EUCFe samples are consistent with the literature in the Central Equatorial Pacific for particulate Fe: 2.01 ± 1.56 ng m^{-3} (2SD, n=11) (GEOTRACES GP15 cruise: between 20° N and 20° S and along the 152° W meridian) (Marsay et al., 2022), 5.60 ± 5.65 ng m^{-3} (2SD, n=8) (P16 cruise of the CLIVAR/CO2 Repeat Hydrography Program: between 9° N and 2° S and along the 151° W meridian) (Landing et al., 2013). The range of EUCFe values was also similar to concentrations in Alaskan coastal and pelagic regions in the subarctic North Pacific, in the North Pacific and in the South Pacific (Buck et al., 2019; Kurisu et al., 2021, 2024; Marsay et al., 2022; Sakata et al., 2022). EUCFe data are lower than aerosol iron concentrations reported in the coastal Northwest Pacific, closer to industrialized areas (Kurisu et al., 2021; Sakata et al., 2022).

The concentrations of the major elements of seawater (Na, Mg, Ca, Sr), and by extension of sea spray, depends on the height of sampling, wave height and wind intensity (Bruch et al., 2021; Madawala et al., 2024). Thus, there is no interest to compare Na, Mg, Ca and Sr concentrations of EUCFe samples with Na, Mg, Ca and Sr concentrations measured in other samples in the Pacific. Therefore, comparing Na, Mg, Ca, and Sr concentrations in EUCFe samples with those measured in other Pacific samples is not meaningful. However, we can compare Al, Ti, V, Zn and Pb elements with the literature. Their concentrations are in the same order of magnitude as those found previously in the atmosphere over the North Pacific (Kurisu et al., 2021, 2024). To the best of our knowledge, the EUCFe Rb, and Ba, La and Ce concentrations are the first measurements over the Pacific Ocean. Their concentrations are similar to those of aerosols over the Atlantic Ocean (Landing and Shelley, 2014; Shelley et al., 2017). Given that V can be used as a tracer of ship's exhaust (Duce and Hoffman, 1976), the lack of correlation between V concentrations and $\delta^{56}Fe$ (Fig. B2) ruled out the possibility of contamination from the ship's exhaust.

Overall, these comparisons are consistent with previous values for these elements and validate the analytical procedure, from sampling to final concentrations.

3.2. IRON ISOTOPIC COMPOSITIONS

EUCFe aAerosols have Fe isotopic ratios ranging from -0.16 ‰ to +0.47 ‰ (Table 3, Fig. 1 and Fig. 3). Those The aerosols sampled along the equator and near close to the Bismarck Sea exhibit have similar, slightly heavy, signatures, ranging from +0.26 ‰ to +0.43 ‰. Those sampled Aerosols in the North Tropical Pacific present more variable signatures, but still positive from +0.14 ‰ to +0.47 ‰. One sample, the southeastern most one (A238), differed significantly from the others in the Equatorial Pacific with the lightest value, -0.16 ‰.

$\delta^{56}Fe$ marine aerosols values from the EUCFe cruise can be compared with three other cruises in the Pacific: KH-13-7 and KH-14-3 in the North Pacific (Kurisu et al., 2021) and GP02 in the subarctic North Pacific (Kurisu et al., 2024) (Fig. 3). In these previous studies, all $\delta^{56}Fe$ values below 0 ‰ were measured in samples taken less than 1,500 km from the Japanese and Alaskan coasts (Fig. 3). In the open ocean, they also reported positive $\delta^{56}Fe$ values as for EUCFe samples (apart from sample A238). South of the tropic of Cancer, Kurisu et al. (2021) reported bulk aerosols heavy $\delta^{56}Fe$ values, between +0.04 ‰ and +0.42 ‰ with a mean value of +0.27 ± 0.26 ‰ (2SD, n=7). In the subarctic North Pacific, the pelagic and Alaskan areas have $\delta^{56}Fe$ values between -0.07 ‰ and +0.45 ‰ (Kurisu et al., 2024). Overall, EUCFe $\delta^{56}Fe$ values are in excellent agreement with these previous works.
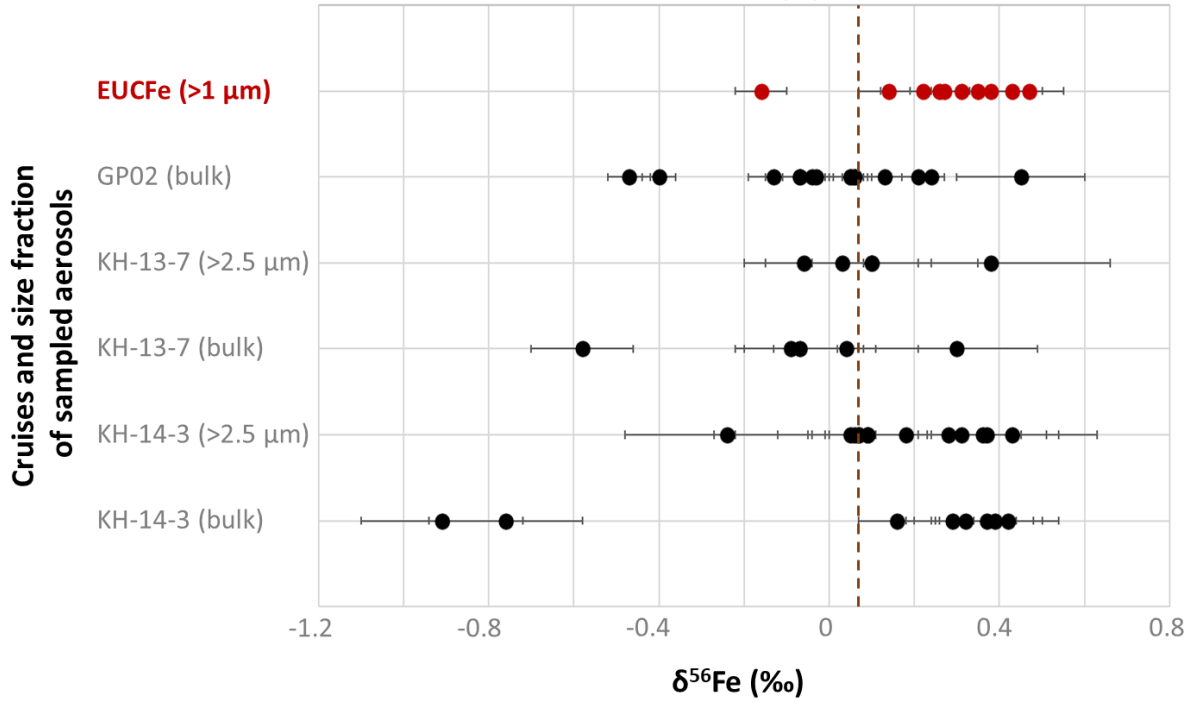
Figure 3. δ^{56}Fe (‰) of sampled aerosols during EUCFe in the Equatorial and Tropical Pacific, GP02 in the subarctic North Pacific (Kurisu et al., 2024), KH-13-7 and KH-14-3 cruises in the North Pacific (Kurisu et al., 2021). Error bars represent 2SD (‰) for EUCFe and GP02 cruises and 2SE (‰) for KH-13-7 and KH-14-3 cruises. 2SE only reflects the dispersions of the MC-ICPMS treatment. The vertical brown line indicates the upper crust value, +0.07 ‰ (Poitrasson, 2006).

4. DISCUSSION

All our marine aerosol samples, except the southeastern one (A238), are enriched in heavy isotopes relative to the crustal value. On average those are characterized by δ^{56}Fe ≈ +0.31 ± 0.21 ‰ (2SD, n=9) (average value except A238, Table 3 and Fig. 1). The value for sample A238 was δ^{56}Fe = -0.16 ‰.

4.1. SOURCES SIGNATURES

First, we will discuss the possibility that aerosol signatures correspond to unmodified source signatures. We will explore three hypotheses: contributions i) from sea spray, ii) from crustal sources, iii) from anthropogenic sources.

A first hypothesis is a contribution from seawater, i.e., sea spray. Based on the assumptions that all Na in EUCFe samples comes from seawater and that the chemical composition of sea spray is that of North Pacific seawater (Nozaki, 1997), the contribution of sea spray to our samples can be estimated with the following equation (Eq. 2).

$$\left[EI_{Sea-spray}\right] = \left[Na_{sample}\right] \frac{[EI_{SW-ref}]}{[Na_{SW-ref}]} \qquad (2)$$

where EI is the element of interest (Fe for instance) and SW-ref is the seawater used as a reference (Nozaki, 1997) for Na and EI (Table 2).

This leads to insignificant contributions from seawater to the Fe content of all our samples (lower than 10^{-5} % of the total Fe content) (Table C1). ~~(< 10^{-56} %) for Fe for all our samples (Table 2).~~ On the other hand, the estimated sea spray contribution for Mg, Ca and Sr was > 89 % for all samples.

A second hypothesis is a source from the erosion products of crustal rocks ~~crustal desert volcanic contribution~~. The crustal signature, δ^{56}Fe = +0.07 ‰, has been characterized in granites (Poitrasson, 2006) but other materials, such as volcanic rocks, exhibit similar isotopic composition. Desert dust, e.g., of Saharan origin, ~~displays crustal signatures~~ (Beard et al., 2003; Waeles et al., 2007; Mead et al., 2013; Conway et al., 2019), as well as basalts (Poitrasson,

2006; Craddock et al., 2013; Teng et al., 2013), display the same signature. ~~Ash, originating from active volcanoes around the Bismarck Sea, have not been directly documented to date to our knowledge, but their signature is likely also crustal, since i)~~ Accordingly, runoff water collected from the flanks of volcano Rabaul in the Bismarck area has been characterized by $\delta^{56}Fe$ = +0.07 ± 0.03 ‰ (2SD, n=2) (Labatut et al., 2014). ~~and ii) Bbasalts also display a crustal signature (Poitrasson, 2006; Craddock et al., 2013; Teng et al., 2013).~~ Therefore, EUCFe aerosol sample isotopic signatures, whether those in the group of nine samples slightly enriched in heavy isotopes or that of the A238 sample slightly enriched in light isotopes, do not directly reflect a crustal source.

A third hypothesis is an anthropogenic origin. Human activities emit aerosols within a wide range of $\delta^{56}Fe$. On the one hand, ~~biomass burning,~~ vehicle exhaust, steel manufacturing, solid waste incineration have been characterized by negative $\delta^{56}Fe$ signatures (~~Mead et al., 2013;~~ Kurisu et al., 2016a~~; Kurisu and Takahashi, 2019~~). On the other hand, coal fly ash, metallic brake dust and steel manufacturing have been characterized by positive $\delta^{56}Fe$ signatures (Flament et al., 2008; Majestic et al., 2009; Mead et al., 2013; Li et al., 2022). Biomass burning can be characterized by both negative $\delta^{56}Fe$ signatures (Mead et al., 2013) and positive $\delta^{56}Fe$ signatures, the latter due to the presence of suspended soil particles (Kurisu and Takahashi, 2019).

Sample A238 ($\delta^{56}Fe$ = -0.16 ‰) is located in the southern part of the Pacific around 140° W (Fig. 1 and Fig. 3, Table 3). The air mass back trajectories (Fig. 2) suggest that aerosols collected in this area originated from the South Pacific or the South American coast. As stated above, several anthropogenic sources, biomass burning, vehicle exhaust, steel manufacturing and solid waste incineration have been characterized by negative signatures (Mead et al., 2013; Kurisu, Sakata, et al., 2016; Kurisu & Takahashi, 2019). Combustion processes from South America are therefore a potential explanation for A238 sample.

The remaining of the discussion will focus on the group of nine samples, characterized by slightly heavy Fe isotopic composition ($\delta^{56}Fe$ = +0.31 ± 0.21 ‰, 2SD, n=9; Fig. 1 and Fig. 3, Table 3). From a purely isotopic signature point of view, anthropogenic sources, e.g., coal combustion and steel manufacturing, possibly mixed with crustal sources, could explain these slightly heavy signatures (Wei et al., 2024). Nevertheless, there are several arguments contradicting this hypothesis: demography, modeled atmospheric back trajectories, aerosol size (> 1 µm) and elemental ratios such as Fe/Ti. While discussing similar slightly heavy aerosol isotopic signatures in the Bismarck Sea, a possible anthropogenic pollution contribution was excluded (Labatut et al., 2014) given the very low demography of the surroundings lands such as Papua New Guinea (Brunskill, 2004). Back trajectories presented in Fig. 2 reveal that the sampled air masses had a wide variety of geographic origins. The fact that aerosols have variable sources but similar isotope signatures does not support the hypothesis of an anthropogenic source such as coal fly ash, metallic brake dust and steel manufacturing, which are not expected to be widely and homogeneously distributed around our study area. The separation between fine and coarse aerosol particles is 2 µm to 2.5 µm (Whitby, 1978; Seinfeld and Pandis, 2006). Nevertheless, fine particles do not ordinarily grow larger than 1 µm (Whitby, 1978). The EUCFe samples are mainly coarse aerosols, a size fraction associated with crustal sources (Mead et al., 2013). The Fe fractional solubility of aerosols was not measured. While this would have been interesting, it is not critical, as this information alone is not necessarily indicative of aerosol sources (Baker and Jickells, 2006; Conway et al., 2015).

The enrichment factor (EF) in an element of interest relative to the crust (Zoller et al., 1974) can be defined as (Eq. 3):

$$\text{Enrichment Factor (EF)} = \frac{\left(\frac{\text{Element of interest}}{\text{Lithogenic tracer}}\right)_{sample}}{\left(\frac{\text{Element of interest}}{\text{Lithogenic tracer}}\right)_{UCC}} \qquad (3)$$

UCC stands for upper continental crust (Rudnick and Gao, 2014) (Table 2). Ti and Al are often used as lithogenic tracers (Dammshäuser, 2012). Because one sample (A252) is suspected to be contaminated in Al (Table 2), we chose Ti to calculate the EF relative to the

crust in the following. Average UCC concentrations are often used as a reference (Rudnick and Gao, 2014). Nevertheless, the UCC exhibits variability in its elemental concentrations, which accounts for the range of Fe/Ti ratios depicted as a grey band in Fig. 4 (Hu and Gao, 2007). This range reflects eight types of rocks (n=40), offering a non exhaustive but more representative overview of the UCC.

Eight of the EUCFe samples fall within the UCC range (Fig. 4). However, two samples exhibit slightly lower (A259) and higher (A266) ratios. Their concentrations of anthropogenic tracers (Pb, V) do not suggest stronger anthropogenic contributions than in the other samples. The Fe/Ti ratios, which fall slightly outside the classical range (Hu & Gao, 2008) in samples A259 and A266, can nonetheless be explained by ultramafic rocks (e.g., pyroxenites), volcanic rocks (e.g., basalts and andesites), metamorphic rocks (e.g., gneiss) or plutonic rocks (e.g., diorite) (Turekian and Wedepohl, 1961; Canil and Lacourse, 2011). These rock types are present around the study area, notably the widespread volcanic rocks (Nusantara, 2000; Neall and Trewick, 2008; Ramos, 2009; Canil and Lacourse, 2011). Thus, despite the variable Fe/Ti ratios in our ten samples, they are all consistent with a crustal origin. Although it is common practice to use Pb or V enrichment factors relative to lithogenic tracers (such as Al or Ti) to trace anthropogenic sources, we chose not to do so because anthropogenic enrichments in Pb or V do not necessarily imply a significant anthropogenic enrichment in Fe ((D1) and Table D2). Their use may therefore be misleading when studying the Fe cycle specifically.

Note that while the Fe/Ti A238 ratio is consistent with a crustal origin, it is also consistent with, for example, biomass burning (Zhai et al., 2021).
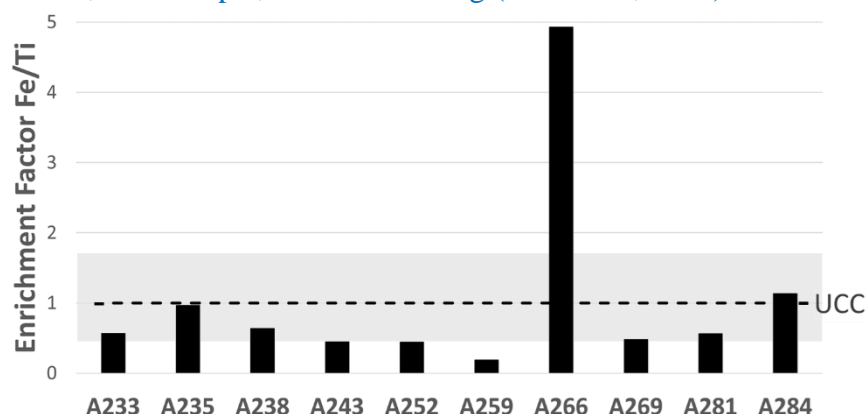

Figure 4. Enrichment factors for Fe relative to Ti in the EUCFe samples, in the UCC reference (dashed line) (Rudnick and Gao, 2014) and in eight UCC types of rocks (grey band) (Hu and Gao, 2008).

~~The EF for Fe/Ti ranges between 0.19 and 4.93 for all samples (Fig. 4). Samples with EFs below 10 are considered natural, without enrichment from an anthropogenic source (Gelado-Caballero et al., 2012).~~ Based on the assumptions that all Ti in EUCFe samples comes from the UCC, and that the chemical composition of crustal aerosol is that of UCC (Rudnick and Gao, 2014) (Table 2), the lithogenic contribution to our samples can be estimated (adjusting Eq. 2 to the case of a lithogenic source). For Fe, this leads to high lithogenic contributions (123 % on average). The fact that this calculation leads to contributions larger than 100 % likely reflects source ratios which differ from that chosen above (UCC) and/or Fe removal during transport.

These arguments, suggest that the slightly heavy iron isotopic compositions are unlikely to be ~~not~~ explained by anthropogenic sources, but mainly by crustal ones. We will discuss below if our observations ($\delta^{56}Fe_{average} = +0.31$ ‰) can be explained by aerosols of crustal origin (+0.07 ‰) which isotopic signature has been modified by isotopic fractionation during atmospheric transport.

13

4.2. ISOTOPIC FRACTIONATION DURING ATMOSPHERIC PROCESSES

A major process influencing aerosol chemistry, during atmospheric transport, is partial dissolution during condensation/evaporation cycles in clouds (Lelieveld and Crutzen, 1991; Desboeufs, 2001). Atmospheric aerosol Fe dissolution is mainly due to dissolution by low pH cloud water and effects of solar irradiation. Different dissolution mechanisms exist, including proton-promoted (Chapman et al., 2009; Kiczka et al., 2010), ligand-promoted (Chapman et al., 2009; Kiczka et al., 2010; Mulholland et al., 2021; Maters et al., 2022), and reductive ligand-promoted dissolution (Mulholland et al., 2021; Maters et al., 2022). Proton-promoted, ligand-controlled and reductive ligand-promoted dissolution are mechanisms happening in clouds (Wiederhold et al., 2006; Maters et al., 2022). These processes fractionate iron isotopes (Mulholland et al., 2021; Maters et al., 2022). In most studies, light iron isotopes are preferentially dissolved, and, the isotopic composition of the remaining particulate iron becomes gradually heavier (Maters et al., 2022) (Fig. 5).
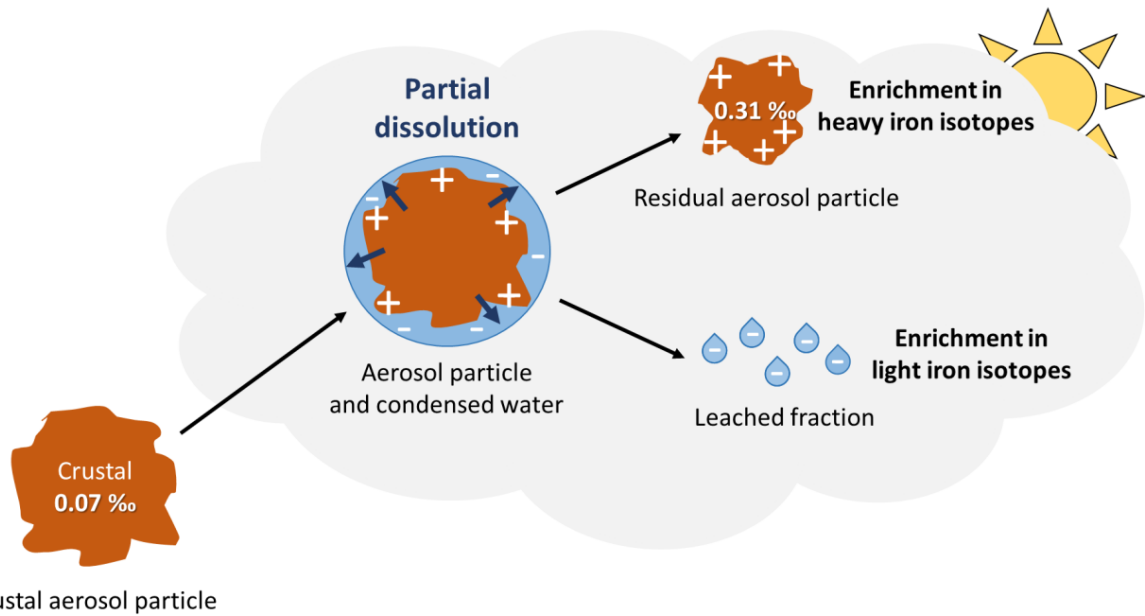

Figure 5. Path of an aerosol during atmospheric transport undergoing partial dissolution. Partial dissolution and subsequent separation of the leached fraction leads the residual particle to an enrichment in heavy and light iron isotopes, in the particles and leached fraction, respectively.

The magnitude of the isotope fractionations, $\Delta^{56}Fe_{solution - particle}$, were found between -0.9 and -1.4 ‰ after biotite and chlorite minerals dissolution (Kiczka et al., 2010) and between -0.4 ± 0.2 ‰ and -1.0 ± 0.15 ‰ (apparent steady state values) after granite and basalts dissolution by hydrochloric acid or oxalic acid (Chapman et al., 2009). An experimentation of anthropogenic aerosols dissolution with synthetic cloud water solution showed light $\delta^{56}Fe$ release ($\Delta^{56}Fe_{solution - particle}$ = -0.284 ± 0.103 ‰) in solution within the first hour of dissolution but heavy $\delta^{56}Fe$ release ($\Delta^{56}Fe_{solution - particle}$ = $+0.227 \pm 0.091$ ‰) in solution after 1 hour (Mulholland et al., 2021). Another experimentation of mineral dust and industrial ash dissolution in simulated cloud water showed a light $\delta^{56}Fe$ enrichment in solution, $\Delta^{56}Fe_{solution - particle}$ between -0.18 ‰ and -0.66 ‰ for ash and between -0.98 ‰ and -1.18 ‰ for dust (Maters et al., 2022). Thus, mineral dissolution appears to favor light isotopes, thereby enriching the remaining solid fraction in heavy isotopes. Therefore, we will assess whether partial dissolution during clouds transport can produce aerosols with a heavier iron isotopic composition. Some authors have suggested that the observed isotopic compositions may be partly due to isotopic fractionation during transport (Kurisu et al., 2021, 2024; Wang et al., 2022).

Considering that the leachate is isolated from the solid fraction of the aerosol, the system can be modeled as a Rayleigh distillation. The isotope composition of the solid fraction of the aerosol is calculated according to Eq. (4) and (5):

$(\delta^{56}Fe_{particle})_f \approx (\delta^{56}Fe_{particle})_{f=1} + \Delta^{56}Fe_{solution - particle} \ln(f)$ (4)

where the particle is the solid fraction of the aerosol, the solution is the leached solution and f is the remaining fraction of $Fe_{particle}$ (when f = 1 all Fe is in the particle; no Fe has been leached). For the particle value, we assume an initial crustal signature for EUCFe aerosols, $(\delta^{56}Fe_{particle})_{f=1}$ = +0.07 ‰ (Poitrasson, 2006). For the isotopic fractionation, $\Delta^{56}Fe_{solution - particle}$, although the experiments described above observed values ranging between -1.4 and +0.23 ‰, we choose -1.8~~1~~ ‰ (Maters et al., 2022). This value was measured during a laboratory experiment on dust with simulated cloud water, i.e., a similar situation to the EUCFe field study (Maters et al., 2022). Equation 5 (derived from Eq. 4) allows us to estimate the fractions of the particles that have to be dissolved (1-f) in order to reach the slightly heavy isotope composition measured.

$1 - f = 1 - e^{\frac{(\delta^{56}Fe_{particle})_{f=1} - (\delta^{56}Fe_{particle})_f}{\Delta^{56}Fe_{solution-particle}}}$ (5)

Based on these calculations, we estimate Fe dissolution percentages varying from 4~~6~~ to 20~~30~~ % with an average value of 13~~20~~ % (Table 4). This is the first estimate of this kind to our knowledge. A comparison can be made with Fe fractional solubility of aerosols measured during seawater or ultrapure deionized water leaching experiments (Sholkovitz et al., 2012; Buck et al., 2013; Shelley et al., 2018; Kurisu et al., 2021, 2024; Desboeufs et al., 2024), keeping in mind that clouds are slightly acidic with a pH around 5 in the Equatorial Pacific (Shah et al., 2020). Locally, Fe fractional solubility can reach ~~52 % in the subarctic North Pacific (Kurisu et al., 2024),~~ 23 % in the Northwestern Pacific (Kurisu et al., 2021) and 29 % in the Pacific Ocean (3 cruises) (Buck et al., 2013) during leaching experiments with ultrapure deionized water. Mean Fe fractional solubility has been reported as the highest in the world in the Equatorial Pacific, with mean values ranging from 12 to 20 % (Hamilton et al., 2019). Fe fractional solubility depends on numerous factors such as aerosols size and origin, atmospheric processes (pH, solar irradiation, composition of the solution). Crustal aerosols collected during dust events in coastal Namibia (aerosols < 10 µm), can reach high Fe fractional solubilities of 20 % (Desboeufs et al., 2024). Therefore, a 13~~20~~ % dissolution is a realistic ~~rather high~~ value for crustal aerosols~~, but is realistic~~.

Table 4. Percentage of Fe dissolution (1-f) necessary to explain the observed EUCFe δ^{56}Fe through atmospheric isotopic fractionation from initial isotope signature of the upper crust (+0.07 ‰). Calculations are performed for all our samples except A238.

Samples	$(\delta^{56}Fe_{particle})_f$ (‰)	1-f (%)
A233	+0.14	~~6~~4
A235	+0.31	~~20~~12
A281	+0.22	~~13~~8
A284	+0.47	~~30~~20
A243	+0.43	~~28~~18
A252	+0.26	~~16~~10
A259	+0.27	~~17~~11
A266	+0.35	~~22~~14
A269	+0.38	~~25~~16
Average of all the above samples	+0.31	~~20~~13

An isotopic fractionation by partial dissolution of crustal origin aerosols could therefore explain the slightly heavy signatures observed (Fig. 5). This would require that the leached fraction, enriched in light isotopes, is separated from the solid fraction. In the absence of separation, the effect of isotope fractionation would not have been measured in our samples. This process has not yet been demonstrated, but the hypothesis has already been proposed in

two publications (Kurisu et al., 2021, 2024). The processes that could lead to such separation are difficult to identify. They are, however, necessary to explain our observations provided that ~~the anthropogenic hypothesis has been rejected~~ aerosol original signatures were crustal. Shattering or ice-breaking are two ways to separate the leached fraction and the residual particle of the aerosols. Their occurrence is understudied especially regarding shattering process. The enrichment of light isotopes in the leached fraction was not observed in this study. This is likely due to the presence of this fraction in aerosols smaller than 1 µm produced by ice-breaking or shattering processes (or its removal by wet deposition), which were not sampled during the EUCFe cruise. The Fe isotopic composition of fine aerosols, often negative, is mostly attributed to anthropogenic sources (Conway et al., 2019; Kurisu et al. 2021). However, this study proposes a new possible cause for the light Fe isotopic composition of aerosols smaller than 1 µm: the residual leached fractions of crustal aerosols. The above model considers the aerosol as a bulk, a homogeneous reservoir. In reality, fractionation occurs at the surface. Taking into account surface processes, would lead to smaller isotopic effects (Wiederhold et al., 2006). Our approximation led to an overestimation of the effect of isotope fractionation and therefore an underestimation of the leached fraction.

5. CONCLUSION

Fe isotope compositions (δ^{56}Fe) and elemental concentrations (Na, Mg, Al, Ca, Ti, Fe, V, ~~Zn,~~ Rb, Sr, Ba~~, La, Ce~~ and Pb) were analyzed in atmospheric particles collected during the EUCFe expedition, in the Equatorial and Tropical Pacific, between Hawaii, the Equator and Papua New Guinea. In all marine aerosol samples with one exception, Fe is enriched in heavy isotopes relative to the crustal value, with an average δ^{56}Fe value of +0.31 ± 0.21 ‰ (2SD, n=9). The simulation of air mass back trajectories, the size of particles, their chemical composition compared to potential sources (enrichment factors) and the geographic environment were used to help explain the enrichment in heavy Fe isotopes. An anthropogenic origin is unlikely ~~was ruled out~~ due to i) the homogeneity aerosols delta values despite a wide variety of modeled geographic origin and ii) the aerosol chemical composition. We conclude that these observations are best explained by crustal aerosols with an initial isotope signature (δ^{56}Fe = +0.07 ‰) modified during atmospheric transport by partial dissolution followed by the removal of the leached fraction. Although such removal had not been previously reported, such Fe isotopes fractionation has been documented in controlled experiments (Mulholland et al., 2021; Maters et al., 2022;) and has already been suggested as one of several explanations for in situ data (Kurisu et al., 2021, 2024). The extent of Fe isotopes fractionation during atmospheric transport requires the dissolution and removal of ~~46~~ to 20~~30~~ % – 13~~20~~ % on average – of the initial aerosol Fe contents.

One aerosol sample stands out by a slightly light isotopic composition of -0.16 ‰, possibly emitted from combustion processes in South America.

This highlights the challenging use of iron isotopes to trace the origin of the aerosols. It also highlights the unique and strong constrains brought by these isotopes on the Fe cycle in atmospheric aerosols. Further studies are needed to confirm the main conclusion of this study, namely the existence of processes leading to the removal of a significant fraction of the iron content of atmospheric aerosols during atmospheric transport.

Authors contributions

J.W.M. was the principal investigator of the EUCFe cruise. F.L. conceived the iron isotope work. A.J. supervised the aerosol collection. M.L., C.P. and FL analyzed the samples. C.C. and F.L. wrote the article. All co-authors reviewed the manuscript.

Competing interests

The authors declare that they have no conflict of interest.

Acknowledges

Financial support

References

Abadie, C., Lacan, F., Radic, A., Pradoux, C., and Poitrasson, F.: Iron isotopes reveal distinct dissolved iron sources and pathways in the intermediate versus deep Southern Ocean, Proceedings of the National Academy of Sciences, 114, 858–863, https://doi.org/10.1073/pnas.1603107114, 2017.

Baker, A. R. and Jickells, T. D.: Mineral particle size as a control on aerosol iron solubility, Geophys Res Lett, 33, https://doi.org/10.1029/2006GL026557, 2006.

Beard, B. L., Johnson, C. M., Von Damm, K. L., and Poulson, R. L.: Iron isotope constraints on Fe cycling and mass balance in oxygenated Earth oceans, Geology, 31, 629–632, https://doi.org/10.1130/0091-7613(2003)031<0629:IICOFC>2.0.CO;2, 2003.

Beard, B. L., Johnson, C. M., Skulan, J. L., Nealson, K. H., Cox, L., and Sun, H.: Application of Fe isotopes to tracing the geochemical and biological cycling of Fe, Chem Geol, 195, 87–117, https://doi.org/10.1016/S0009-2541(02)00390-X, 2003.

Boyd, P. W. and Ellwood, M. J.: The biogeochemical cycle of iron in the ocean, Nature Geosci, 3, 675–682, https://doi.org/10.1038/ngeo964, 2010.

Boyle, E. A., John, S., Abouchami, W., Adkins, J. F., Echegoyen-Sanz, Y., Ellwood, M., Flegal, A. R., Fornace, K., Gallon, C., Galer, S., Gault-Ringold, M., Lacan, F., Radic, A., Rehkamper, M., Rouxel, O., Sohrin, Y., Stirling, C., Thompson, C., Vance, D., Xue, Z., and Zhao, Y.: GEOTRACES IC1 (BATS) contamination-prone trace element isotopes Cd, Fe, Pb, Zn, Cu, and Mo intercalibration, Limno Oceanogr-Meth, 10, 653–665, https://doi.org/10.4319/lom.2012.10.653, 2012.

Bruch, W., Piazzola, J., Branger, H., van Eijk, A. M. J., Luneau, C., Bourras, D., and Tedeschi, G.: Sea-Spray-Generation Dependence on Wind and Wave Combinations: A Laboratory Study, Bound-Lay Meteorol, 180, 477–505, https://doi.org/10.1007/s10546-021-00636-y, 2021.

Brunskill, G. J.: New Guinea and its coastal seas, a testable model of wet tropical coastal processes: an introduction to Project TROPICS, Cont Shelf Res, 24, 2273–2295, https://doi.org/10.1016/j.csr.2004.08.001, 2004.

Buck, C. S., Landing, W. M., and Resing, J.: Pacific Ocean aerosols: Deposition and solubility of iron, aluminum, and other trace elements, Mar Chem, 157, 117–130, https://doi.org/10.1016/j.marchem.2013.09.005, 2013.

Buck, C. S., Aguilar-Islas, A., Marsay, C., Kadko, D., and Landing, W. M.: Trace element concentrations, elemental ratios, and enrichment factors observed in aerosol samples collected during the US GEOTRACES eastern Pacific Ocean transect (GP16), Chem Geol, 511, 212–224, https://doi.org/10.1016/j.chemgeo.2019.01.002, 2019.

Canil, D. and Lacourse, T.: An estimate for the bulk composition of juvenile upper continental crust derived from glacial till in the North American Cordillera, Chem Geol, 284, 229–239, https://doi.org/10.1016/j.chemgeo.2011.02.024, 2011.

Chapman, J. B., Weiss, D. J., Shan, Y., and Lemburger, M.: Iron isotope fractionation during leaching of granite and basalt by hydrochloric and oxalic acids, Geochim Cosmochim Ac, 73, 1312–1324, https://doi.org/10.1016/j.gca.2008.11.037, 2009.

Chen, T., Li, W., Guo, B., Liu, R., Li, G., Zhao, L., and Ji, J.: Reactive iron isotope signatures of the East Asian dust particles: Implications for iron cycling in the deep North Pacific, Chem Geol, 531, 119342, https://doi.org/10.1016/j.chemgeo.2019.119342, 2020.

Conway, T. M. and John, S. G.: Quantification of dissolved iron sources to the North Atlantic Ocean, Nature, 511, 212–215, https://doi.org/10.1038/nature13482, 2014.

Conway, T. M., Wolff, E. W., Röthlisberger, R., Mulvaney, R., and Elderfield, H. E.: Constraints on soluble aerosol iron flux to the Southern Ocean at the Last Glacial Maximum, Nat Commun, 6, 7850, https://doi.org/10.1038/ncomms8850, 2015.

Conway, T. M., John, S. G., and Lacan, F.: Intercomparison of dissolved iron isotope profiles from reoccupation of three GEOTRACES stations in the Atlantic Ocean, Mar Chem, 183, 50–61, https://doi.org/10.1016/j.marchem.2016.04.007, 2016.

Conway, T. M., Hamilton, D. S., Shelley, R. U., Aguilar-Islas, A. M., Landing, W. M., Mahowald, N. M., and John, S. G.: Tracing and constraining anthropogenic aerosol iron fluxes to the North Atlantic Ocean using iron isotopes, Nat Commun, 10, 2628, https://doi.org/10.1038/s41467-019-10457-w, 2019.

Craddock, P. R., Warren, J. M., and Dauphas, N.: Abyssal peridotites reveal the near-chondritic Fe isotopic composition of the Earth, Earth Planet Sc Lett, 365, 63–76, https://doi.org/10.1016/j.epsl.2013.01.011, 2013.

Dammshäuser, A.: Distribution and behavior of the lithogenic tracers aluminium and titanium in the upper water column of the Atlantic Ocean, Faculty of Mathematics and Natural Sciences Christian-Albrechts-Universität zu Kiel, 2012.

Desboeufs, K.: Processus de dissolution des aérosols atmosphériques au sein des gouttes d'eau nuageuses, Université Paris-Diderot - Paris VII, 2001.

Desboeufs, K., Formenti, P., Torres-Sánchez, R., Schepanski, K., Chaboureau, J.-P., Andersen, H., Cermak, J., Feuerstein, S., Laurent, B., Klopper, D., Namwoonde, A., Cazaunau, M., Chevaillier, S., Feron, A., Mirande-Bret, C., Triquet, S., and Piketh, S. J.: Fractional solubility of iron in mineral dust aerosols over coastal Namibia: a link to marine biogenic emissions?, Atmos Chem Phys, 24, 1525–1541, https://doi.org/10.5194/acp-24-1525-2024, 2024.

Duce, R. A. and Hoffman, G. L.: Atmospheric vanadium transport to the ocean, Atmos Environ, 10, 989–996, https://doi.org/10.1016/0004-6981(76)90207-9, 1976.

Duce, R. A. and Tindale, N. W.: Atmospheric transport of iron and its deposition in the ocean, Limnol Oceanogr, 36, 1715–1726, https://doi.org/10.4319/lo.1991.36.8.1715, 1991.

Elrod, V. A., Berelson, W. M., Coale, K. H., and Johnson, K. S.: The flux of iron from continental shelf sediments: A missing source for global budgets, Geophys Res Lett, 31, https://doi.org/10.1029/2004GL020216, 2004.

Ellwood, M. J., Hutchins, D. A., Lohan, M. C., Milne, A., Nasemann, P., Nodder, S. D., Sander, S. G., Strzepek, R., Wilhelm, S. W., and Boyd, P. W.: Iron stable isotopes track pelagic iron cycling during a subtropical phytoplankton bloom, P Natl Acad Sci USA, 112, E15–E20, https://doi.org/10.1073/pnas.1421576112, 2015.

Flament, P., Mattielli, N., Aimoz, L., Choël, M., Deboudt, K., Jong, J. de, Rimetz-Planchon, J., and Weis, D.: Iron isotopic fractionation in industrial emissions and urban aerosols, Chemosphere, 73, 1793–1798, https://doi.org/10.1016/j.chemosphere.2008.08.042, 2008.

Gelado-Caballero, M. D., López-García, P., Prieto, S., Patey, M. D., Collado, C., and Hérnández-Brito, J. J.: Long-term aerosol measurements in Gran Canaria, Canary Islands: Particle concentration, sources and elemental composition, J Geophys Res-Atmos, 117, https://doi.org/10.1029/2011JD016646, 2012.

Hamilton, D. S., Scanza, R. A., Feng, Y., Guinness, J., Kok, J. F., Li, L., Liu, X., Rathod, S. D., Wan, J. S., Wu, M., and Mahowald, N. M.: Improved methodologies for Earth system modelling of atmospheric soluble iron and observation comparisons using the Mechanism of Intermediate complexity for Modelling Iron (MIMI v1.0), Geosci Model Dev, 12, 3835–3862, https://doi.org/10.5194/gmd-12-3835-2019, 2019.

Hao, Y., Guo, Z., Yang, Z., Fang, M., and Feng, J.: Seasonal variations and sources of various elements in the atmospheric aerosols in Qingdao, China, Atmos Res, 85, 27–37, https://doi.org/10.1016/j.atmosres.2006.11.001, 2007.

Homoky, W. B., Conway, T. M., John, S. G., König, D., Deng, F., Tagliabue, A., and Mills, R. A.: Iron colloids dominate sedimentary supply to the ocean interior, P Natl Acad Sci USA, 118, e2016078118, https://doi.org/10.1073/pnas.2016078118, 2021.

Hu, Z. and Gao, S.: Upper crustal abundances of trace elements: A revision and update, Chem Geol, 253, 205–221, https://doi.org/10.1016/j.chemgeo.2008.05.010, 2008.

Jickells, T., An, Z., Andersen, K., Baker, A., Bergametti, G., Brooks, N., Cao, J., Boyd, P., Duce, R., Hunter, K., Kawahata, H., Kubilay, N., Laroche, J., Liss, P., Mahowald, N., Prospero, J., Ridgwell, A., Tegen, I., and Torres, R.: Global Iron Connections Between Desert Dust, Ocean Biogeochemistry, and Climate, Science (New York, N.Y.), 308, 67–71, https://doi.org/10.1126/science.1105959, 2005.

John, S. G., Mendez, J., Moffett, J., and Adkins, J.: The flux of iron and iron isotopes from San Pedro Basin sediments, Geochim Cosmochim Ac, 93, 14–29, https://doi.org/10.1016/j.gca.2012.06.003, 2012.

Kiczka, M., Wiederhold, J. G., Frommer, J., Kraemer, S. M., Bourdon, B., and Kretzschmar, R.: Iron isotope fractionation during proton- and ligand-promoted dissolution of primary phyllosilicates, Geochim Cosmochim Ac, 74, 3112–3128, https://doi.org/10.1016/j.gca.2010.02.018, 2010.

Klar, J. K., Schlosser, C., Milton, J. A., Woodward, E. M. S., Lacan, F., Parkinson, I. J., Achterberg, E. P., and James, R. H.: Sources of dissolved iron to oxygen minimum zone waters on the Senegalese continental margin in the tropical North Atlantic Ocean: Insights from iron isotopes, Geochim Cosmochim Ac, 236, 60–78, https://doi.org/10.1016/j.gca.2018.02.031, 2018.

Kommalapati, R. R. and Valsaraj, K. T.: Atmospheric Aerosols and Their Importance, in: Atmospheric Aerosols, vol. 1005, American Chemical Society, 1–10, https://doi.org/10.1021/bk-2009-1005.ch001, 2009.

Kurisu, M. and Takahashi, Y.: Testing Iron Stable Isotope Ratios as a Signature of Biomass Burning, Atmosphere-Basel, 10, 76, https://doi.org/10.3390/atmos10020076, 2019.

Kurisu, M., Sakata, K., Miyamoto, C., Takaku, Y., Iizuka, T., and Takahashi, Y.: Variation of Iron Isotope Ratios in Anthropogenic Materials Emitted through Combustion Processes, Chem Lett, 45, 970–972, https://doi.org/10.1246/cl.160451, 2016a.

Kurisu, M., Takahashi, Y., Iizuka, T., and Uematsu, M.: Very low isotope ratio of iron in fine aerosols related to its contribution to the surface ocean, J Geophys Res-Atmos, 121, 11,119-11,136, https://doi.org/10.1002/2016JD024957, 2016b.

Kurisu, M., Sakata, K., Uematsu, M., Ito, A., and Takahashi, Y.: Contribution of combustion Fe in marine aerosols over the northwestern Pacific estimated by Fe stable isotope ratios, Atmos Chem Phys, 21, 16027–16050, https://doi.org/10.5194/acp-21-16027-2021, 2021.

Kurisu, M., Sakata, K., Nishioka, J., Obata, H., Conway, T. M., Hunt, H. R., Sieber, M., Suzuki, K., Kashiwabara, T., Kubo, S., Takada, M., and Takahashi, Y.: Source and fate of atmospheric iron supplied to the subarctic North Pacific traced by stable iron isotope ratios, Geochim Cosmochim Ac, 378, 168–185, https://doi.org/10.1016/j.gca.2024.06.009, 2024.

Labatut, M., Lacan, F., Pradoux, C., Chmeleff, J., Radic, A., Murray, J. W., Poitrasson, F., Johansen, A. M., and Thil, F.: Iron sources and dissolved-particulate interactions in the seawater of the Western Equatorial Pacific, iron isotope perspectives, Global Biogeochem Cy, 28, 1044–1065, https://doi.org/10.1002/2014GB004928, 2014.

Lacan, F., Radic, A., Jeandel, C., Poitrasson, F., Sarthou, G., Pradoux, C., and Freydier, R.: Measurement of the isotopic composition of dissolved iron in the open ocean, Geophys Res Lett, 35, L24610, https://doi.org/10.1029/2008GL035841, 2008.

Lacan, F., Radic, A., Labatut, M., Jeandel, C., Poitrasson, F., Sarthou, G., Pradoux, C., Chmeleff, J., and Freydier, R.: High-Precision Determination of the Isotopic Composition of Dissolved Iron in Iron Depleted Seawater by Double Spike Multicollector-ICPMS, Anal. Chem., 82, 7103–7111, https://doi.org/10.1021/ac1002504, 2010.

Lacan, F., Artigue, L., Klar, J. K., Pradoux, C., Chmeleff, J., and Freydier, R.: Interferences and Matrix Effects on Iron Isotopic Composition Measurements by 57Fe-58Fe Double-Spike Multi-Collector Inductively Coupled Plasma Mass Spectrometry; the Importance of Calcium and Aluminum Interferences, Front Environ Chem, 2, https://doi.org/10.3389/fenvc.2021.692025, 2021.

Landing, W. M. and Shelley, R.: Total aerosol trace metal concentrations from R/V Knorr cruises KN199-04 and KN204-01 in the Subtropical northern Atlantic Ocean from 2010-2011 (U.S. GEOTRACES NAT project) (Version 16 September 2014), http://lod.bco-dmo.org/id/dataset/3865, 2014.

Landing, W. M., Measures, C. I., and Resing, J. A.: Collaborative Research: Global Ocean Survey of Dissolved Iron and Aluminum and Aerosol Iron and Aluminum Solubility Supporting the Repeat Hydrography (CO2) Project (CLIVAR AEROSOL) (Version 12 June 2013), 2013.

Lelieveld, J. and Crutzen, P. J.: The role of clouds in tropospheric photochemistry, J Atmos Chem, 12, 229–267, https://doi.org/10.1007/BF00048075, 1991.

Li, R., Zhang, H., Wang, F., He, Y., Huang, C., Luo, L., Dong, S., Jia, X., and Tang, M.: Mass fractions, solubility, speciation and isotopic compositions of iron in coal and municipal waste fly ash, Sci Total Environ, 838, 155974, https://doi.org/10.1016/j.scitotenv.2022.155974, 2022.

Madawala, C. K., Molina, C., Kim, D., Gamage, D. K., Sun, M., Leibensperger, R. J. I., Mehndiratta, L., Lee, J., Kaluarachchi, C. P., Kimble, K. A., Sandstrom, G., Harb, C., Dinasquet, J., Malfatti, F., Prather, K. A., Deane, G. B., Stokes, M. D., Lee, C., Slade, J. H., Stone, E. A., Grassian, V. H., and Tivanski, A. V.: Effects of Wind Speed on Size-Dependent Morphology and Composition of Sea Spray Aerosols, ACS Earth Space Chem, 8, 1609–1622, https://doi.org/10.1021/acsearthspacechem.4c00119, 2024.

Majestic, B. J., Anbar, A. D., and Herckes, P.: Elemental and iron isotopic composition of aerosols collected in a parking structure, Sci Total Environ, 407, 5104–5109, https://doi.org/10.1016/j.scitotenv.2009.05.053, 2009.

Marsay, C. M., Kadko, D., Landing, W. M., and Buck, C. S.: Bulk Aerosol Trace Element Concentrations and Deposition Fluxes During the U.S. GEOTRACES GP15 Pacific Meridional Transect, Global Biogeochem Cy, 36, e2021GB007122, https://doi.org/10.1029/2021GB007122, 2022.

Martin, J. H.: Iron as a Limiting Factor in Oceanic Productivity, in: Primary Productivity and Biogeochemical Cycles in the Sea, edited by: Falkowski, P. G., Woodhead, A. D., and Vivirito, K., Springer, Boston, MA, 123–137, https://doi.org/10.1007/978-1-4899-0762-2_8, 1992.

Maters, E. C., Mulholland, D. S., Flament, P., de Jong, J., Mattielli, N., Deboudt, K., Dhont, G., and Bychkov, E.: Laboratory study of iron isotope fractionation during dissolution of mineral dust and industrial ash in simulated cloud water, Chemosphere, 299, 134472, https://doi.org/10.1016/j.chemosphere.2022.134472, 2022.

Mead, C., Herckes, P., Majestic, B. J., and Anbar, A. D.: Source apportionment of aerosol iron in the marine environment using iron isotope analysis, Geophys Res Lett, 40, 5722–5727, https://doi.org/10.1002/2013GL057713, 2013.

Moore, J. K. and Braucher, O.: Sedimentary and mineral dust sources of dissolved iron to the world ocean, Biogeosciences, 5, 631–656, https://doi.org/10.5194/bg-5-631-2008, 2008.

Morel, F. M. M., Lam, P. J., and Saito, M. A.: Trace Metal Substitution in Marine Phytoplankton, Annu Rev Earth Pl Sc, 48, 491–517, https://doi.org/10.1146/annurev-earth-053018-060108, 2020.

Mulholland, D. S., Flament, P., de Jong, J., Mattielli, N., Deboudt, K., Dhont, G., and Bychkov, E.: In-cloud processing as a possible source of isotopically light iron from anthropogenic aerosols: New insights from a laboratory study, Atmos Environ, 259, 118505, https://doi.org/10.1016/j.atmosenv.2021.118505, 2021.

Neall, V. E. and Trewick, S. A.: The age and origin of the Pacific islands: a geological overview, Philos T Roy Soc B, 363, 3293–3308, https://doi.org/10.1098/rstb.2008.0119, 2008.

Nozaki, Y.: A fresh look at element distribution in the North Pacific Ocean, Eos, Transactions American Geophysical Union, 78, 221–221, https://doi.org/10.1029/97EO00148, 1997.

Nusantara, L.: An outline of the geology of Indonesia., Ikatan Ahli Geologi Indonesia, 2000.

Poitrasson, F.: On the iron isotope homogeneity level of the continental crust, Chem Geol, 235, 195–200, https://doi.org/10.1016/j.chemgeo.2006.06.010, 2006.

Poulton, S. W. and Raiswell, R.: The low-temperature geochemical cycle of iron: From continental fluxes to marine sediment deposition, Am J Sci, 302, 774–805, https://doi.org/10.2475/ajs.302.9.774, 2002.

Radic, A., Lacan, F., and Murray, J. W.: Iron isotopes in the seawater of the equatorial Pacific Ocean: New constraints for the oceanic iron cycle, Earth Planet Sc Lett, 306, 1–10, https://doi.org/10.1016/j.epsl.2011.03.015, 2011.

Raiswell, R., Benning, L. G., Tranter, M., and Tulaczyk, S.: Bioavailable iron in the Southern Ocean: the significance of the iceberg conveyor belt, Geochem T, 9, 7, https://doi.org/10.1186/1467-4866-9-7, 2008.

Ramos, V. A.: Anatomy and global context of the Andes: Main geologic features and the Andean orogenic cycle, in: Backbone of the Americas: Shallow Subduction, Plateau Uplift, and Ridge and Terrane Collision, edited by: Kay, S. M., Ramos, V. A., and Dickinson, W. R., Geological Society of America, 0, https://doi.org/10.1130/2009.1204(02), 2009.

Resing, J. A., Sedwick, P. N., German, C. R., Jenkins, W. J., Moffett, J. W., Sohst, B. M., and Tagliabue, A.: Basin-scale transport of hydrothermal dissolved metals across the South Pacific Ocean, Nature, 523, 200–203, https://doi.org/10.1038/nature14577, 2015.

Rudnick, R. L. and Gao, S.: 4.1 - Composition of the Continental Crust, in: Treatise on Geochemistry (Second Edition), edited by: Holland, H. D. and Turekian, K. K., Elsevier, Oxford, 1–51, https://doi.org/10.1016/B978-0-08-095975-7.00301-6, 2014.

Sakata, K., Kurisu, M., Takeichi, Y., Sakaguchi, A., Tanimoto, H., Tamenori, Y., Matsuki, A., and Takahashi, Y.: Iron (Fe) speciation in size-fractionated aerosol particles in the Pacific Ocean: The role of organic complexation of Fe with humic-like substances in controlling Fe solubility, Atmos Chem Phys, 22, 9461–9482, https://doi.org/10.5194/acp-22-9461-2022, 2022.

Seinfeld, J. H. and Pandis, S. N.: Atmospheric Chemistry and Physics: From Air Pollution to Climate Change, John Wiley & Sons, 2006.

Shah, V., Jacob, D. J., Moch, J. M., Wang, X., and Zhai, S.: Global modeling of cloud water acidity, precipitation acidity, and acid inputs to ecosystems, Atmos Chem Phys, 20, 12223–12245, https://doi.org/10.5194/acp-20-12223-2020, 2020.

Shelley, R. U., Roca-Martí, M., Castrillejo, M., Sanial, V., Masqué, P., Landing, W. M., van Beek, P., Planquette, H., and Sarthou, G.: Quantification of trace element atmospheric deposition fluxes to the Atlantic Ocean (>40°N; GEOVIDE, GEOTRACES GA01) during spring 2014, Deep Sea Research Part I: Oceanographic Research Papers, 119, 34–49, https://doi.org/10.1016/j.dsr.2016.11.010, 2017.

Shelley, R. U., Landing, W. M., Ussher, S. J., Planquette, H., and Sarthou, G.: Regional trends in the fractional solubility of Fe and other metals from North Atlantic aerosols (GEOTRACES cruises GA01 and GA03) following a two-stage leach, Biogeosciences, 15, 2271–2288, https://doi.org/10.5194/bg-15-2271-2018, 2018.

Sholkovitz, E. R., Sedwick, P. N., Church, T. M., Baker, A. R., and Powell, C. F.: Fractional solubility of aerosol iron: Synthesis of a global-scale data set, Geochim Cosmochim Ac, 89, 173–189, https://doi.org/10.1016/j.gca.2012.04.022, 2012.

Slemons, L., Gorgues, T., Aumont, O., Menkes, C., and Murray, J. W.: Biogeochemical impact of a model western iron source in the Pacific Equatorial Undercurrent, Deep-Sea Res Pt I, 56, 2115–2128, https://doi.org/10.1016/j.dsr.2009.08.005, 2009.

Slemons, L., Murray, J. W., Resing, J., Paul, B., and Dutrieux, P.: Western Pacific coastal sources of iron, manganese, and aluminum to the Equatorial Undercurrent, Global Biogeochem Cy, 24, https://doi.org/10.1029/2009GB003693, 2010.

Slemons, L., Paul, B., Resing, J., and Murray, J. W.: Particulate iron, aluminum, and manganese in the Pacific equatorial undercurrent and low latitude western boundary current sources, Mar Chem, 142–144, 54–67, https://doi.org/10.1016/j.marchem.2012.08.003, 2012.

Stein, A. F., Draxler, R. R., Rolph, G. D., Stunder, B. J. B., Cohen, M. D., and Ngan, F.: NOAA's HYSPLIT Atmospheric Transport and Dispersion Modeling System, B Am Meteorol Soc, 96, 2059–2077, https://doi.org/10.1175/BAMS-D-14-00110.1, 2015.

Tagliabue, A., Bopp, L., Dutay, J.-C., Bowie, A. R., Chever, F., Jean-Baptiste, P., Bucciarelli, E., Lannuzel, D., Remenyi, T., Sarthou, G., Aumont, O., Gehlen, M., and Jeandel, C.: Hydrothermal contribution to the oceanic dissolved iron inventory, Nature Geosci, 3, 252–256, https://doi.org/10.1038/ngeo818, 2010.

785 Teng, F.-Z., Dauphas, N., Huang, S., and Marty, B.: Iron isotopic systematics of oceanic basalts,
786   Geochim Cosmochim Ac, 107, 12–26, https://doi.org/10.1016/j.gca.2012.12.027, 2013.
787 Tovar-Sánchez, A., Arrieta, J. M., Duarte, C. M., and Sañudo-Wilhelmy, S. A.: Spatial gradients in trace
788   metal concentrations in the surface microlayer of the Mediterranean Sea, Front. Mar. Sci., 1,
789   https://doi.org/10.3389/fmars.2014.00079, 2014.
790 Turekian, K. K. and Wedepohl, K. H.: Distribution of the Elements in Some Major Units of the Earth's
791   Crust, GSA Bulletin, 72, 175–192, https://doi.org/10.1130/0016-
792   7606(1961)72[175:DOTEIS]2.0.CO;2, 1961.
793 Waeles, M., Baker, A. R., Jickells, T., and Hoogewerff, J.: Global dust teleconnections: aerosol iron
794   solubility and stable isotope composition, Environ Chem, 4, 233,
795   https://doi.org/10.1071/EN07013, 2007.
796 Wang, Y., Wu, L., Hu, W., Li, W., Shi, Z., Harrison, R. M., and Fu, P.: Stable iron isotopic composition of
797   atmospheric aerosols: An overview, npj Clim Atmos Sci, 5, 1–13, https://doi.org/10.1038/s41612-
798   022-00299-7, 2022.
799 Wei, T., Dong, Z., Zong, C., Liu, X., Kang, S., Yan, Y., and Ren, J.: Global-scale constraints on the origins
800   of aerosol iron using stable iron isotopes: A review, Earth-Sci Rev, 258, 104943,
801   https://doi.org/10.1016/j.earscirev.2024.104943, 2024.
802 Whitby, K. T.: The physical characteristics of sulfur aerosols, Atmos Environ, 12, 135–159,
803   https://doi.org/10.1016/0004-6981(78)90196-8, 1978.
804 Wiederhold, J. G., Kraemer, S. M., Teutsch, N., Borer, P. M., Halliday, A. N., and Kretzschmar, R.: Iron
805   Isotope Fractionation during Proton-Promoted, Ligand-Controlled, and Reductive Dissolution of
806   Goethite, Environ. Sci. Technol., 40, 3787–3793, https://doi.org/10.1021/es052228y, 2006.
807 Wunderman, R.: Report on Rabaul (Papua New Guinea), Bulletin of the Global Volcanism Network,
808   31, https://doi.org/10.5479/si.GVP.BGVN200609-252140, 2006.
809 Yeghicheyan, D., Bossy, C., Bouhnik Le Coz, M., Douchet, C., Granier, G., Heimburger, A., Lacan, F.,
810   Lanzanova, A., Rousseau, T. C. C., Seidel, J.-L., Tharaud, M., Candaudap, F., Chmeleff, J., Cloquet,
811   C., Delpoux, S., Labatut, M., Losno, R., Pradoux, C., Sivry, Y., and Sonke, J. E.: A Compilation of
812   Silicon, Rare Earth Element and Twenty-One other Trace Element Concentrations in the Natural
813   River Water Reference Material SLRS-5 (NRC-CNRC), Geostand Geoanal Res, 37, 449–467,
814   https://doi.org/10.1111/j.1751-908X.2013.00232.x, 2013.
815 Yeghicheyan, D., Aubert, D., Bouhnik-Le Coz, M., Chmeleff, J., Delpoux, S., Djouraev, I., Granier, G.,
816   Lacan, F., Piro, J.-L., Rousseau, T., Cloquet, C., Marquet, A., Menniti, C., Pradoux, C., Freydier, R.,
817   Vieira da Silva-Filho, E., and Suchorski, K.: A New Interlaboratory Characterisation of Silicon, Rare
818   Earth Elements and Twenty-Two Other Trace Element Concentrations in the Natural River Water
819   Certified Reference Material SLRS-6 (NRC-CNRC), Geostand Geoanal Res, 43, 475–496,
820   https://doi.org/10.1111/ggr.12268, 2019.
821 Zhai, J., Burke, I. T., Mayes, W. M., and Stewart, D. I.: New insights into biomass combustion ash
822   categorisation: A phylogenetic analysis, Fuel, 287, 119469,
823   https://doi.org/10.1016/j.fuel.2020.119469, 2021.
824 Zoller, W. H., Gladney, E. S., and Duce, R. A.: Atmospheric Concentrations and Sources of Trace
825   Metals at the South Pole, Science, 183, 198–200, https://doi.org/10.1126/science.183.4121.198,
826   1974.
827

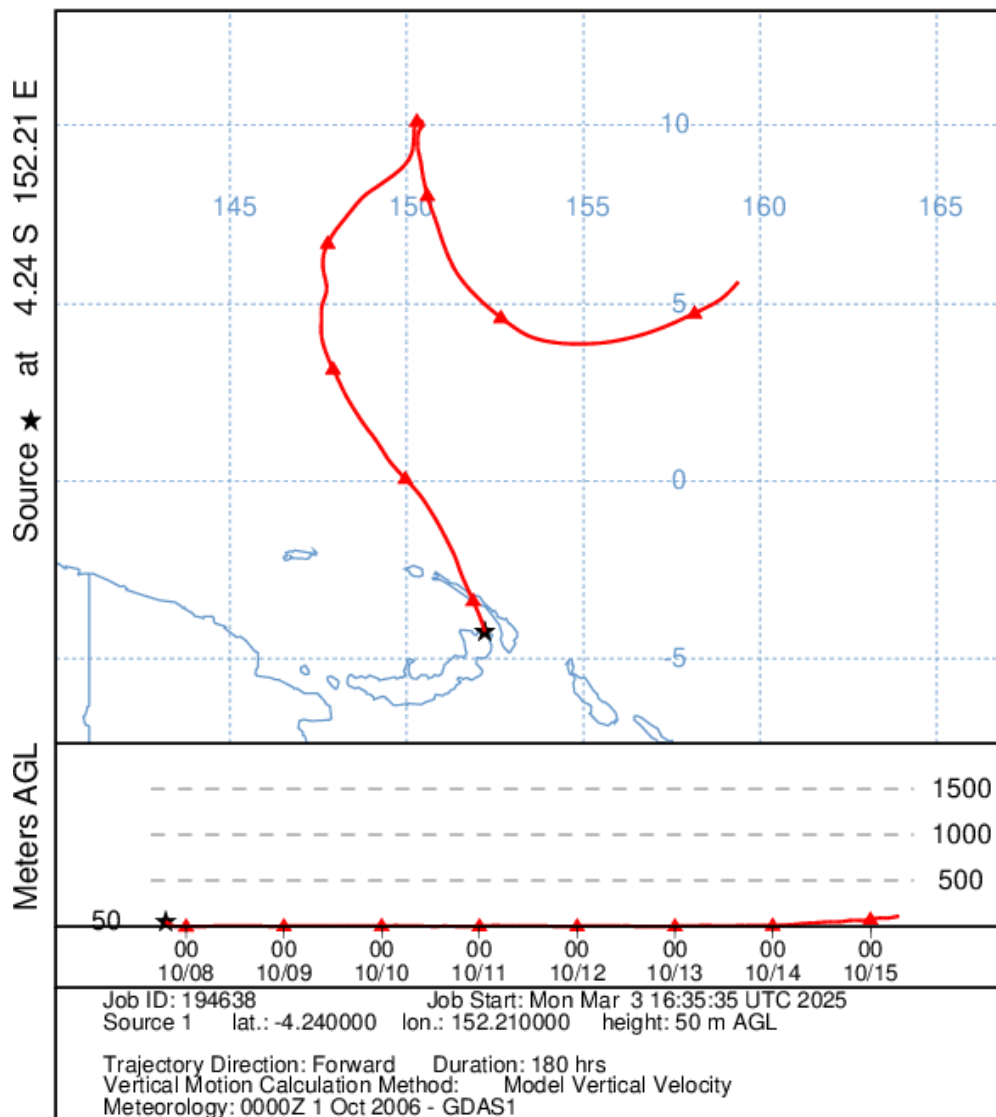828 **Appendices**
829 **Appendix A.**

Fig. A1. Air mass forward trajectory (red line) calculated with Hybrid Single-Particle Lagrangian Integrated Trajectory model (HYSPLIT, NOAA, GDSA Meteorological Data). Trajectory was conducted at the height of 50 m (AGL) with a 7.5 days run time. The starting point of the trajectory is the Tavurvur volcano at 9 am (PGT, UTC+10) on 7 October 2006, when the eruption began (Wunderman, 2006).
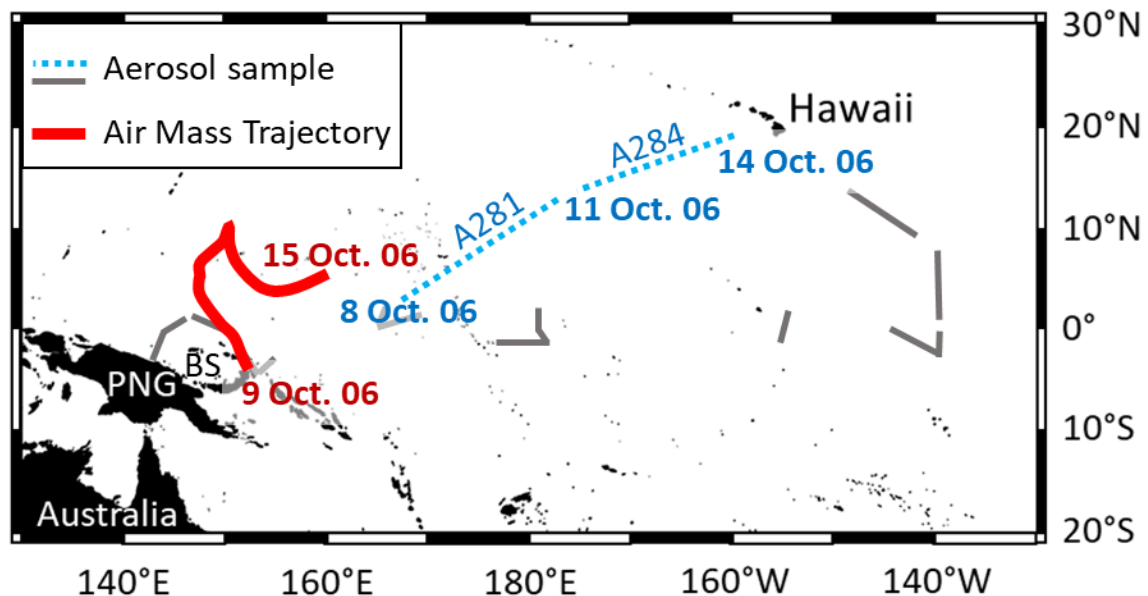
838
839 **Fig. A2.** Reproduction on the forward trajectory (Fig. S1) on the aerosol sampling map. The
840 starting point of the forward trajectory is the Tavurvur volcano at 9 am (PGT, UTC+10) on 7
841 October 2006, when the eruption began (Wunderman, 2006). The ending point of the trajectory
842 is on 15 October 2006. Aerosol samples in color (A281 and A284) are the only samples
843 collected after the eruption, between 8 October 2006 and 14 October 2006. PNG stands for
844 Papua New Guinea. BS stands for Bismarck Sea.
845
846 **Appendix B.**
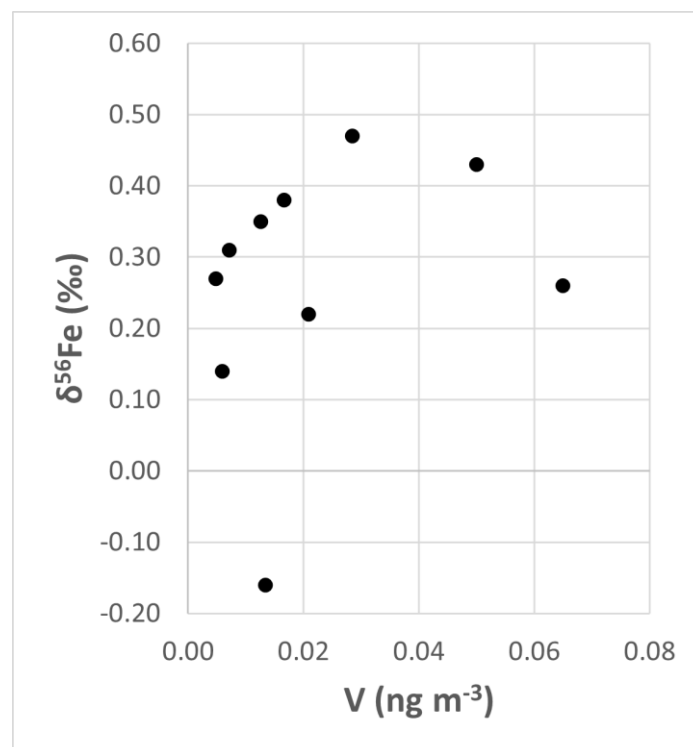
847
848 **Fig. B1.** Fe isotopic composition (δ^{56}Fe) and Vanadium (V) concentrations of EUCFe aerosol
849 samples.
850
851 **Appendix C.**
852 **Table C1.** Na concentrations (ng m^{-3}) and contribution of sea spray (%) to the Fe content of
853 EUCFe samples.
854

Samples ID	[Na] (ng m^{-3})	Fe from sea spray (%)
A233	17.5	2.19 x 10^{-7}
A235	128	4.18 x 10^{-7}
A238	323	2.21 x 10^{-6}
A243	114	1.25 x 10^{-6}
A252	223	6.84 x 10^{-6}
A259	77.6	5.92 x 10^{-6}
A266	20	1.12 x 10^{-7}
A269	12.5	6.23 x 10^{-7}
A281	58.6	7.51 x 10^{-7}
A284	97.7	5.77 x 10^{-7}

855

856 **Appendix D.**

857 **(D1).** Calculation of the relative contribution of two sources, from elemental mass ratios (e.g.,
858 Pb/Fe)

859 In the hypothesis of a 2 end-member mixing, when the mass ratios of two elements are known
860 in the two sources and in the mixture, **then the contribution of each source to the mixture**
861 **can be calculated for the two elements.**

862

863 Below the two sources are named "source 1" and "source 2" and the mixture is named "sample".

864 QPb and QFe are quantities (ng) and [Pb] and [Fe] are concentrations (ng m^{-3}).

865

866 $\frac{QPb}{QFe}$ sample, $\frac{QPb}{QFe}$ source 1, $\frac{QPb}{QFe}$ source 2 are known.

867 2 end-member mixing implies: $\frac{QPb}{QFe}$ sample $= \frac{QPb\ source\ 1 + QPb\ source\ 2}{QFe\ source\ 1 + QFe\ source\ 2}$

868 This is equivalent to $\frac{QPb}{QFe}$ sample $= \frac{QFe\ source\ 1 * \frac{QPb\ source\ 1}{QFe\ source\ 1} + QFe\ source\ 2 * \frac{QPb\ source\ 2}{QFe\ source\ 2}}{QFe\ source\ 1 + QFe\ source\ 2}$

869 With, $x = \frac{QFe\ source\ 1}{QFe\ source\ 2}$ mass ratio in the sample.

870

871 $$\frac{QPb}{QFe}\ sample = \frac{QFe\ source\ 1 * \frac{QPb\ source\ 1}{QFe\ source\ 1} + \frac{QFe\ source\ 1}{x} * \frac{QPb\ source\ 2}{QFe\ source\ 2}}{QFe\ source\ 1 + \frac{QFe\ source\ 1}{x}}$$

872

873 This is equivalent to $$\frac{QPb}{QFe}\ sample = \frac{\frac{QPb\ source\ 1}{QFe\ source\ 1} + \frac{1}{x} * \frac{QPb\ source\ 2}{QFe\ source\ 2}}{1 + \frac{1}{x}}$$

874

875 Therefore, $$x = \frac{\left(\frac{QPb}{QFe}\right) sample - \left(\frac{QPb}{QFe}\right) source\ 2}{\left(\frac{QPb}{QFe}\right) source\ 1 - \left(\frac{QPb}{QFe}\right) sample}$$

876

877 With this formula, we can calculate the anthropogenic and crustal contributions for both Fe and
878 Pb, in our samples given that the ratios are known in the 2 sources.

879

880 Below we illustrate our point with an example. For the anthropogenic source, we used data
881 from Hao et al. (2007). This study was chosen for three main reasons: (1) the study area is
882 relevant to our research - Qingdao, China (550 km from Beijing), a city with 2.3 million
883 inhabitants; (2) the authors explicitly identify Pb as representing pollution and Fe as indicative
884 of soil sources; and (3) the study provides elemental concentrations for each sample, allowing
885 us to calculate Pb/Fe mass ratios, unlike most studies that only report mean concentrations. For
886 the crustal source, we used the average of ratios found in eight different types of rocks from the
887 UCC (Hu and Gao, 2008). The element ratios of these sources are 0.00095 g g^{-1} for the crustal
888 source and 0.182 g g^{-1} for the anthropogenic source (roughly 200 times higher than the UCC).
889 We applied these calculations to EUCFe samples and results are shown in Table D2.

890

891 **Table D2.** Contribution of the anthropogenic source to Fe and Pb content of EUCFe samples
892 (% w w[-1]). The element ratios of the UCC source is 0.00095 g g^{-1} (Hu and Gao, 2008) and 0.182
893 g g^{-1} for the anthropogenic source (Hao et al., 2007).

Contribution (%w w[-1]) of the anthropogenic source to the content of:	EUCFe samples										
	A233	A235	A238	A243	A252	A259	A266	A269	A281	A284	Average
Fe	3 %	1 %	2 %	ND	7 %	15 %	ND	20 %	6 %	4 %	7 %
Pb	86 %	53 %	79 %	ND	94 %	97 %	ND	98 %	93 %	89 %	86 %

894